ACS APPLIED BIO MATERIALS

www.acsabm.org

Article

Highly Sensitive Electrochemical Immunosensor Platforms for Dual Detection of SARS-CoV-2 Antigen and Antibody based on Gold Nanoparticle Functionalized Graphene Oxide Nanocomposites

Mohd. Abubakar Sadique, Shalu Yadav, Pushpesh Ranjan, Raju Khan,* Firoz Khan, Ashok Kumar, and Debasis Biswas

Cite This: *ACS Appl. Bio Mater.* 2022, 5, 2421−2430

Read Online

ACCESS | Metrics & More | Article Recommendations | Supporting Information

ABSTRACT: In this work, we report a facile synthesis of graphene oxide−gold (GO−Au) nanocomposites by electrodeposition. The fabricated electrochemical immunosensors are utilized for the dual detection of severe acute respiratory syndrome coronavirus 2 (SARS-CoV-2) antigen and SARS-CoV-2 antibody. The GO−Au nanocomposites has been characterized by UV−vis spectroscopy, X-ray diffraction (XRD), transmission electron microscopy (TEM), cyclic voltammetry (CV), differential pulse voltammetry (DPV), and electrochemical impedance spectroscopy (EIS) for its biosensing properties. The linear detection range of the SARS-CoV-2 antigen immunosensor is 10.0 ag mL^{-1} to 50.0 ng mL^{-1}, whereas that for the antibody immunosensor ranges from 1.0 fg mL^{-1} to 1.0 ng mL^{-1}. The calculated limit of detection (LOD) of the SARS-CoV-2 antigen immunosensor is 3.99 ag mL^{-1}, and that for SARS-CoV-2 antibody immunosensor is 1.0 fg mL^{-1} with high sensitivity. The validation of the immunosensor has also been carried out on patient serum and patient swab samples from COVID-19 patients. The results suggest successful utilization of the immunosensors with a very low detection limit enabling its use in clinical samples. Further work is needed for the standardization of the results and translation in screen-printed electrodes for use in portable commercial applications.

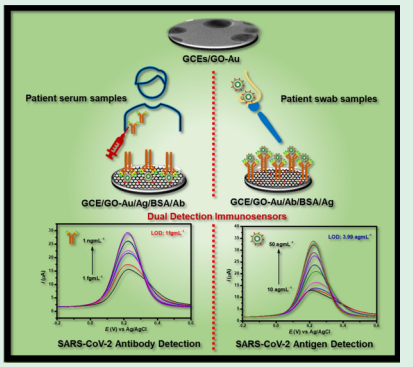

KEYWORDS: *SARS-CoV-2 antigen, SARS-CoV-2 antibody, GO−Au nanocomposites, electrodeposition, electrochemical immunosensor*

1. INTRODUCTION

Humanity has always been ravaged by numerous viral diseases from ancient history to modern times. Several infectious viruses, such as influenza,[1] middle east respiratory syndrome coronavirus (MERS),[2] and severe acute respiratory syndrome coronavirus (SARS-CoV), have led to global outbreaks. The current pandemic has caused a huge loss of life, wealth, and necessities, which encouraged the scientific community to develop some prevention and treatment strategies.[3] One of the most essential preventive measures is an accurate, rapid, and sensitive diagnostic platform.[4] This can be an effective tool to combat pandemics and outbreaks and even enable early detection of the disease in places where high-throughput methods are needed for a huge population.[5] The current ongoing outbreak of coronavirus 2019 (COVID-19) disease was caused by SARS-CoV-2, which emerged at the end of 2019. To date, the virus has evolved with various strains and variants of concern that have bypassed the conventional diagnostic tools.[6]

Presently, the typical solution for the detection of SARS-CoV-2 is reverse transcriptase-polymerase chain reaction (RT-PCR), which provides highly sensitive and accurate results by detecting genomic molecules like RNA. However, expensive setup, the requirement for trained personnel, sample contamination, false-positive results, etc., limit its applicability for diagnosis of COVID-19.[7] Similarly, serological methods such as enzyme-linked immunosorbent assay (ELISA) detect antibodies against viral SARS-CoV-2 antigens, but these methods involve tedious and time-consuming procedures that restrict their further applicability in mass testing of SARS-CoV-2. For rapid on-site detection, such methods lack the advantages of biosensors. The complex methodology, expensive instrumentation, time-consuming procedures, and insensitive analysis of conventional methods restricts fulfilling high testing demand, which requires rapid, inexpensive, sensitive, and early detection. Accordingly, biosensors can provide effective solutions for such public demands.[8]

The main requirements are lower detection limit, no-cross reactivity, high sensitivity, clinical sample analysis, and rapid and accurate results with point of care (POC) testing.[9] Several POC biosensors, such as fluorescence-based, field-effect

Received: April 2, 2022
Accepted: April 21, 2022
Published: May 6, 2022

https://doi.org/10.1021/acsabm.2c00301
ACS Appl. Bio Mater. 2022, 5, 2421−2430

Scheme 1. Schematic of Steps Involved in the Fabrication of SARS-CoV-2 Antigen and SARS-CoV-2 Antibody Immunosensors

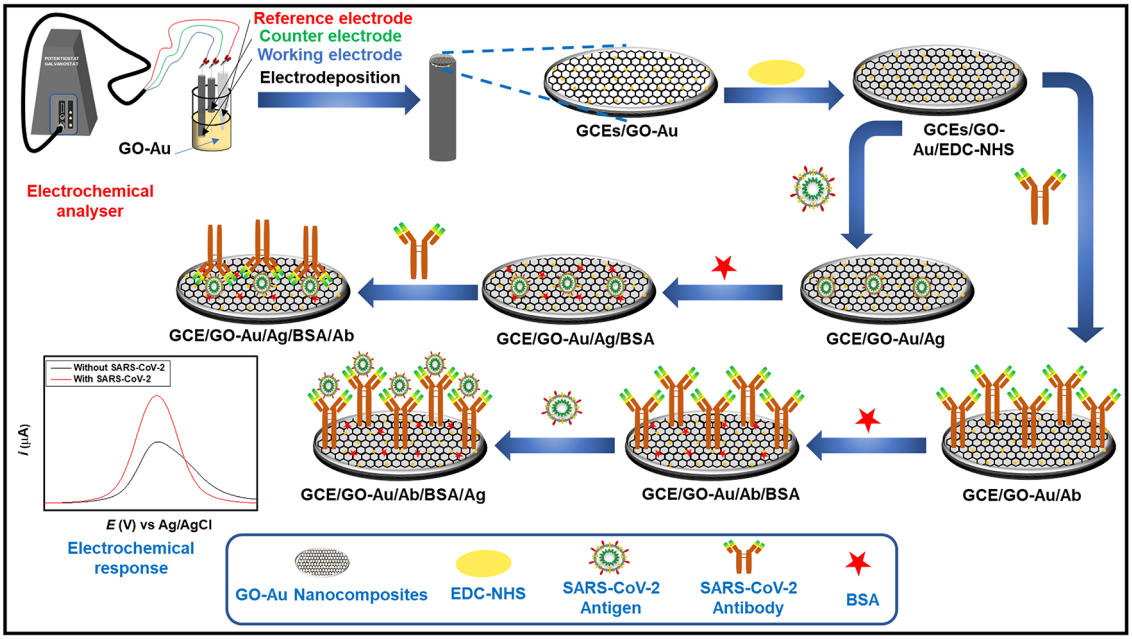

transistor (FET)-based,[10,11] and electrochemical-based biosensors, have been reported for the detection of SARS-CoV-2 with various enabling nanomaterials. Among these, electrochemical biosensors have advantages over other conventional methods due to their high sensitivity, ease of operation, rapid detection, portability, environmental stability, selectivity, and simple working principles, though the development of electrochemical biosensors with superior transducing capabilities, high active surface area, and functionalities needs to be explored.

Recent studies on electrochemical biosensors have explored the potential of numerous nanomaterials and their nanocomposites, especially gold nanoparticles (AuNPs) due to their high conductivity, high surface area, and superior binding capabilities with biomolecules.[12] Similarly, several carbon nanomaterials, such as graphene oxide (GO) or reduced graphene oxide (RGO), have also been utilized in biosensing applications owing to their remarkable surface functionality, high biocompatibility, and electrical conductivity.[13] Pristine GO has low conductivity, and its defect-free synthesis is still a challenge. Alternatively, the combination of GO and AuNPs provides feasible synthesis and favorable characteristics for electrochemical biosensing applications. AuNPs have been one of the most utilized metal nanoparticles in electrochemical biosensors due to their significant features, such as high conductivity, strong adsorption capability, and biocompatibility.[14] Additionally, AuNPs prevent stacking of graphene oxide sheets and enhance stability, active surface area, and interface for biomolecule immobilization.

Among other synthesis routes, electrochemical deposition has several advantages such as being swift, facile, ecofriendly, simple, and convenient and having easy handling and high stability. Also, it provides in situ reductions of both GO and AuNPs on the surface of the working electrode.[15]

Previously, several electrochemical platforms have been reported for the detection of SARS-CoV-2 antigen and antibodies. For instance, Alafeef et al. fabricated a graphene−Au based electrochemical biosensor with LOD of 6.9 copies μL^{-1}.[6] Zhao et al. developed a highly sensitive graphene−Au sandwich-type electrochemical platform with LOD of 200 copies mL^{-1}.[16] The Hashemi group reported LOD up to 1.68×10^{-22} μg mL^{-1} for a GO−Au based electrochemical system.[17] Yakoh and co-workers reported a highly sensitive paper-based electrochemical platform with a detection limit of 1 ng mL^{-1}.[18] Ali et al. developed an aerosol jet nanoprinted RGO-coated 3D electrode-based electrochemical system having a LOD of 2.8×10^{-15} M.[19]

In this work, a facile synthesis route for GO−Au nanocomposites is described along with the fabrication of two immunosensors for the dual detection of SARS-CoV-2 antigen and SARS-CoV-2 antibody. The synthesized GO−Au nanocomposites has remarkable properties for sensing applications because of the large surface area, high conductivity, and availability of functional groups for effective biomolecule binding. Both immunosensors were successfully utilized for SARS-CoV-2 detection through the highly sensitive differential pulse voltammetry (DPV) technique. The dual detection of both the immunosensors was carried out in redox electrolyte with synthetic samples and later validated with patient serum as well as nasopharyngeal swab samples. The obtained LOD for the SARS-CoV-2 antigen immunosensor is 3.99 ag mL^{-1}, while that for the SARS-CoV-2 antibody immunosensor is ∼1.0 fg mL^{-1}. The results show that the fabricated immunosensors have great potential for accurate, rapid, reliable, and sensitive detection of SARS-CoV-2 antigen, as well as SARS-CoV-2 antibody, in clinical point-of-care (POC) applications.

2. EXPERIMENTAL SECTION

2.1. Instruments, Materials, and Reagents. Recombinant human SARS-CoV-2 nucleocapsid protein expressed in *Escherichia coli* (His tag) (ab273530) (SARS-CoV-2 antigen), and anti-nucleocapsid SARS-CoV-2 immunoglobulin (Ig) G (ab273167) (SARS-CoV-2 antibody) were procured from Abcam, UK. Graphite (powder), hydrogen tetrachloroaurate(III) ($HAuCl_4 \cdot 3H_2O$), potassium ferricyanide(III) [$K_3Fe(CN)_6$], potassium hexacyanoferrate trihydrate [$K_4Fe(CN)_6 \cdot 3H_2O$], *N*-(3-(dimethylamino)propyl)-*N*′-

https://doi.org/10.1021/acsabm.2c00301
ACS Appl. Bio Mater. 2022, 5, 2421−2430

ethyl carbodiimide hydrochloride (EDC), *N*-hydroxysulfosuccinimide sodium salt (NHS), and bovine serum albumin (BSA) were purchased from Sigma-Aldrich, USA. Sodium phosphate monobasic dihydrate ($NaH_2PO_4{\cdot}2H_2O$), sodium phosphate dibasic (Na_2HPO_4), potassium chloride (KCl), sodium hydroxide (NaOH), and potassium permanganate ($KMnO_4$) were purchased from Merck, India. Hydrogen peroxide (H_2O_2; ∼30.0%) was purchased from Central Drug House (P) Ltd. (CDH), India. Sulfuric acid (H_2SO_4), *ortho*-phosphoric acid (H_3PO_4), and hydrochloric acid (HCl) were purchased from RANKEM. All remaining solvents were of laboratory grade, and reagents and chemicals were of analytical grade and were used without purification. All solutions were prepared in ultrapure milli-Q water (18.3 MΩ) from a Millipore instrument.

The synthesized GO, GO−Au nanocomposites, and modified electrodes were characterized for their optical, elemental, structural, and electrochemical properties using UV−visible spectroscopy (Evolution 220 UV−vis spectrophotometer, Thermo Fisher Scientific), X-ray diffraction (Rigaku Miniflex-1; Cu Kα radiation, λ = 1.54 Å), transmission electron microscopy (JEOL, JEM-F200; analysis performed at 200 keV), and electrochemical analysis (Autolab potentiostat/galvanostat electrochemical analyzer; Metrohm, PGSTAT204), respectively.

2.2. Synthesis of Graphene Oxide. GO was prepared by the previously reported modified Hummer's method with slight modifications.[20,21] The detailed methodology is given in Supporting Information.

2.3. Pretreatment of the Working Electrode. A glassy carbon electrode (GCE) was used as the working electrode for further modifications. The GCE was cleaned before use as per the methodology described in the Supporting Information.

2.4. Fabrication of GO−Au Nanocomposites Modified Electrode. For the fabrication of the GO−Au nanocomposites modified electrode, GO was dispersed in milli-Q water through ultrasonication for 30 min at a concentration of 0.05 mg mL^{-1}. The electrodeposition solution was prepared by mixing 0.5 M H_2SO_4, 4 mM $HAuCl_4{\cdot}3H_2O$, and 0.05 mg mL^{-1} GO in 10 mL of milli-Q water. The electrodeposition solution was ultrasonicated for 1 h. An electrochemical analyzer was used to perform the electrodeposition on the GCE via the cyclic voltammetry (CV) technique in the above solution using a 3-electrode system, GCE as the working electrode, Pt wire as the counter electrode, and Ag/AgCl (3 M KCl) as the reference electrode. For electrodeposition, the applied potential window was in the range −0.2 to +1.2 V at a scan rate of 20 mV/s for 15 cycles to obtain a uniform thickness of the deposited film.[22] The simultaneous reduction of GO and $HAuCl_4$ resulted in the formation of the GO−Au nanocomposites film on the working electrode surface. The surface-modified working electrode was rinsed with milli-Q water and dried at room temperature (25 °C) for further characterization and modifications.[23] The fabrication of the GO−Au nanocomposites on a GCE by electrodeposition is shown in Scheme 1.

2.5. Fabrication of SARS-CoV-2 Antibody and SARS-CoV-2 Antigen Immunosensors. After electrochemical investigation of the GO−Au nanocomposites modified GCE electrode, it was treated by drop-casting with 5 μL of EDC/NHS, 4:1, solution for 2 h at room temperature activating carboxylic groups at the termini.[22] The electrode was rinsed with phosphate-buffered saline (PBS, pH 7.0) to remove the unbound reagents. For the fabrication of the SARS-CoV-2 antibody immunosensor, with 5 μL of the SARS-CoV-2 antigen (5 μg mL^{-1}) (in PBS, pH 7.4) was drop cast onto the surface activated electrode (GCE/GO−Au/Ag) and incubated overnight at 4°C. Alternatively, for the fabrication of the SARS-CoV-2 antigen immunosensor, 5 μL of the SARS-CoV-2 antibody (5 μg mL^{-1} in PBS, pH 7.4) was drop cast onto the surface activated electrode and incubated under similar conditions. Then both the electrodes were rinsed with PBS (pH 7.0) to remove excess or unbound proteins.[24] The electrodes were again electrochemically characterized to confirm the binding of proteins on the modified GCE surface. After characterization, the electrode was again rinsed with PBS (pH 7.0). In the final step, both electrodes were treated by drop-casting with 5 μL of 0.1% BSA in PBS (pH 7.0) and incubated for 1 h to block unbound free sites on the surface of the electrode (GCE/GO−Au/Ag/BSA and GCE/GO−Au/Ab/BSA). The electrodes were rinsed and electrochemically characterized. Finally, the SARS-CoV-2 antibody and SARS-CoV-2 antigen immunosensors were ready for detection studies.[25] The fabrication steps of SARS-CoV-2 antibody and SARS-CoV-2 antigen immunosensors are depicted in Scheme 1.

2.6. Morphological Analysis and Electrochemical Measurements. The synthesized GO, GO−Au nanocomposites, and modified electrodes were characterized for their optical, elemental, vibrational, structural, and electrochemical properties using UV−visible spectroscopy, XRD, FT-IR, TEM, and an Autolab potentiostat/galvanostat electrochemical analyzer, respectively. After each surface modification step, the electrochemical measurements were conducted using CV and DPV using the applied potential window in the range of −0.3 to +0.8 V, the scan rate of 20 mV/s, and electrochemical impedance spectroscopy (EIS) in the frequency range of 0.1 to 1 MHz using a three-electrode system with glassy carbon electrode as working electrode, Pt wire as counter electrode, and Ag/AgCl (3 M KCl) as reference electrode. The electrolyte used for all the measurements was 0.1 M PBS (pH 7.4) containing 5 mM ferri/ferrocyanide and 0.1 M KCl (later referred to as "redox electrolyte").

2.7. Detection and Clinical Sample Preparation. Serum samples were obtained from the CSIR-Cohort serosurvey conducted at CSIR-AMPRI (Bhopal). COVID-19 RT-PCR positive and negative nasopharyngeal swab samples (N = 9) were received from the Department of Microbiology, All India Institute of Medical Sciences (AIIMS), Bhopal. The project was approved by the Institutional Human Ethics Committee (IHEC) and the Institutional Biosafety Committee (IBSC). Nasopharyngeal swab samples were handled in the Biosafety Level III (BSL-III) biocontainment facility of AIIMS Bhopal.

The samples used for detection of SARS-CoV-2 antibody and SARS-CoV-2 antigen have been prepared as follows:

The synthetic SARS-CoV-2 antibody detection samples were prepared from the 5 μg mL^{-1} stock solution of SARS-CoV-2 antibody in PBS (pH 7.2). Various concentration dilutions were made ranging from 1 fg mL^{-1} to 1 ng mL^{-1} in redox electrolyte. The samples were kept at −20 °C before further use. The synthetic SARS-CoV-2 antigen samples were prepared from the 50 μg mL^{-1} stock solution of SARS-CoV-2 antigen in PBS (pH 7.2). Various concentration dilutions were made ranging from 10 ag mL^{-1} to 50 ng mL^{-1} in the redox electrolyte. The samples were kept at −20 °C before further use. Patient serum samples for SARS-CoV-2 antibody detection were acquired from the serosurvey and used after 1:9 dilution in redox electrolyte. The solutions were kept at −20 °C before further use. Patient nasopharyngeal swab samples were inactivated in the BSL-III lab with Triton X-100 (0.5%) solution and stored in viral transport medium (VTM, 0.5%) at −20 °C before further use. The inactivated samples were diluted in redox electrolyte at a 1:9 ratio and stored at −20 °C before further use.

3. RESULTS AND DISCUSSION

The final synthesized nanocomposites and fabricated immunosensors were characterized by various techniques for verification and validation of the work. The nanocomposites was characterized using UV−vis spectroscopy, X-ray diffraction (XRD), and (TEM) characterization techniques. Furthermore, the fabricated immunosensors were characterized by CV, differential pulse voltammetry (DPV), and electrochemical impedance spectroscopy (EIS) techniques.

3.1. Structural Analysis of the GO−Au Nanocomposites. For initial confirmation of nanocomposites formation, primary characterization was done by XRD. The characteristic peaks of GO were observed at 12.1° with interplanar spacing (d) of 1.46 nm. The presence of a peak at 26.4°, which corresponds to RGO, shows that the GO was partially reduced. The peak of RGO corresponds to the (002) plane with d = 0.20 nm. The GO has a hexagonal carbon structure (JCPDS

https://doi.org/10.1021/acsabm.2c00301
ACS Appl. Bio Mater. 2022, 5, 2421−2430

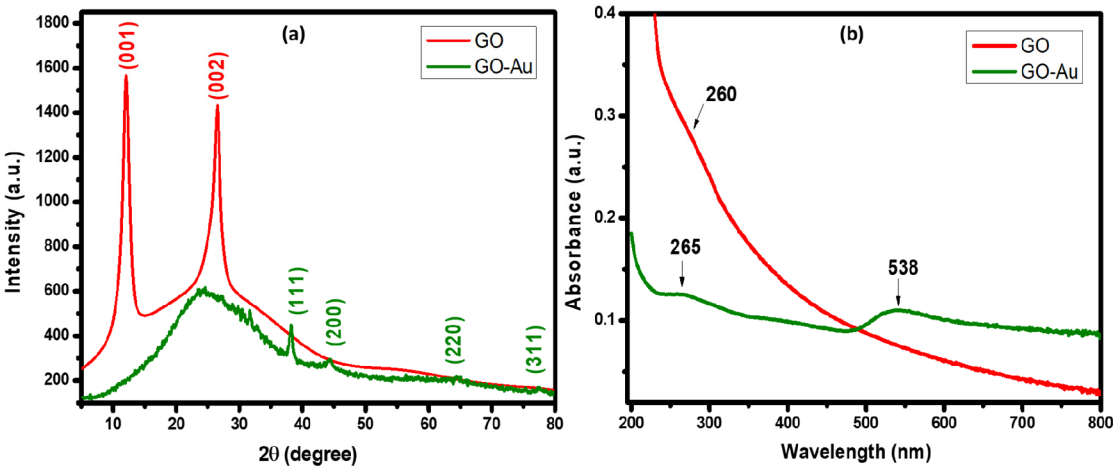

Figure 1. (a) XRD spectra and (b) UV−vis spectra of GO nanosheets (red) and GO−Au nanocomposites (green).

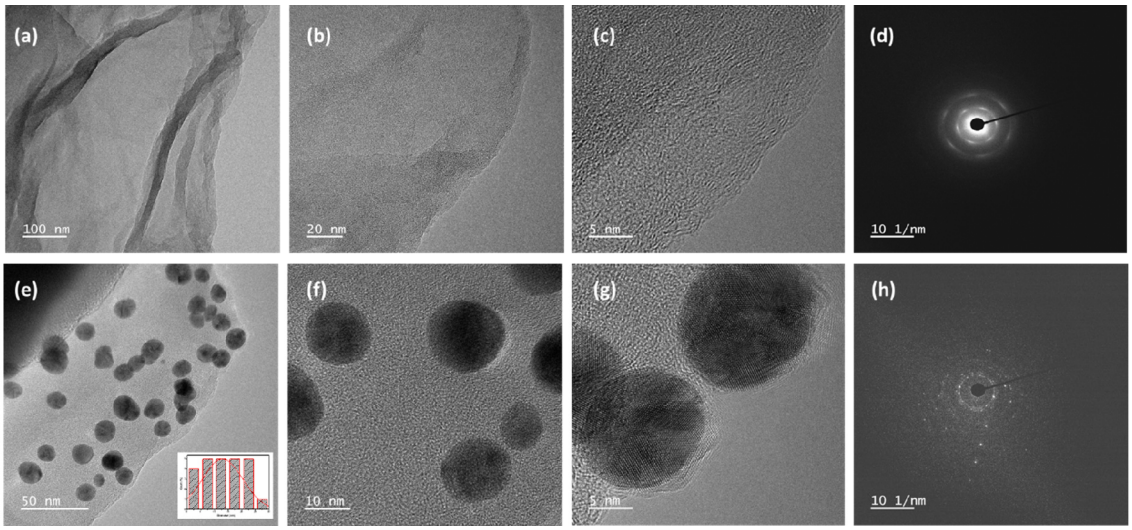

Figure 2. TEM images of (a−c) GO nanosheets and (e−g) GO−Au nanocomposites (inset of panel e, particle distribution graph of AuNPs). SAED patterns of (d) GO nanosheets and (h) GO−Au nanocomposites.

Card No. 75-1621) with restacked layers of graphene and the presence of a peak at 12.1° indicating the presence of oxygen functionalities.[26] In the case of the GO−Au nanocomposites, the peaks of GO and RGO at 12.1° and 26.4° merged, and a broad peak was observed at 24.5°. The characteristic peaks of Au were observed at 38.2°, 44.4°, 64.4°, and 77.5° for the planes (111), (200), (220), and (311), respectively, confirming its crystalline nature (JCPDS 04-0784).[27] The corresponding *d* values for planes (111), (200), (220), and (311) is 0.47, 0.40, 0.28, and 0.24 nm, respectively. The disappearance of the peak at 12.1° shows the reduction of GO to RGO. The appearance of a peak at 24.5° in the GO−Au nanocomposites suggests the successful attachment of AuNPs on the surface of GO.[28] The obtained results confirmed the formation of the GO−Au nanocomposites as shown in Figure 1a.

3.2. Optical Study of the GO−Au Nanocomposites. The basic characterization of the nanocomposites was carried out by UV−vis spectroscopy, which gave primary confirmation of the successful synthesis of the GO and GO−Au nanocomposites. The absorption peak of GO is observed at 265 nm corresponding to the presence of aromatic C═C bonds which have $\pi-\pi^*$ transition in the sp^2 carbon framework.[29] Further, in the case of the GO−Au nanocomposites, characteristic peaks of both GO (265 nm) and Au (538 nm) are observed.[30] The peak at 538 nm is characteristic of AuNPs due to their surface plasmonic resonance effect. The results confirm the formation of the GO−Au nanocomposites (Figure 1b).

3.3. Morphological Studies of GO−Au Nanocomposites. The structural and morphological analysis of the synthesized GO and GO−Au nanocomposites was done by TEM. A wrinkled sheet-like pattern was observed at the 100 nm scale, and a thin sheet is visible at the 20 nm scale for the synthesized GO nanosheets (Figure 2a−c). For the GO−Au nanocomposites (Figure 2e−g), a clear indication of uniform dispersion of AuNPs verified the formation of the nanocomposites.[31] The high-resolution TEM images (Figure 2c,g) clearly show the interplanar and interatomic spacing of GO nanosheets and AuNPs, respectively. The selected area electron diffraction (SAED) pattern of GO nanosheets is shown in Figure 2d, where the presence of diffused spots shows the semicrystalline nature of GO nanosheets. The presence of concentric rings along with clear spots suggests the polycrystalline nature of the GO−Au nanocomposites in Figure 2h. The inset of Figure 2e shows the particle distribution graph of AuNPs, where the average particle size is calculated to be 12.5 nm.

https://doi.org/10.1021/acsabm.2c00301
ACS Appl. Bio Mater. 2022, 5, 2421−2430

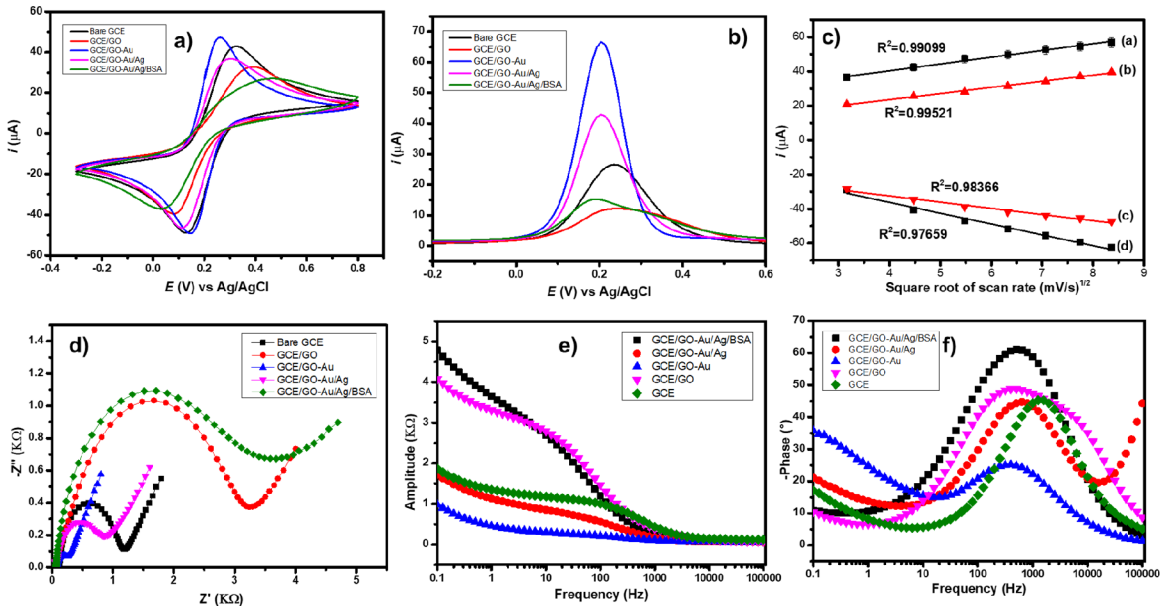

Figure 3. Comparative electrochemical characterization via (a) CV, (b) DPV, (c) scan rate study, (d) Nyquist plot, and (e, f) Bode plots of bare GCE, GCE/GO, GCE/GO−Au, GCE/GO−Au/Ag, and GCE/GO−Au/Ag/BSA modified SARS-CoV-2 antibody immunosensor.

3.4. Electrochemical Performance of the GO−Au Nanocomposites and Fabricated Immunosensors. A detailed analysis of the electrochemical activity has been carried out on the synthesized nanocomposites, surface modified electrodes, and fabricated immunosensors before utilizing them for detection of the SARS-CoV-2 antibody and SARS-CoV-2 antigen. The immunosensors were initially characterized by CV, DPV, and EIS. All electrochemical measurements were performed in redox electrolyte and measured against the reference Ag/AgCl (3 M KCl) electrode.

CV was utilized to characterize the electrode at each stage of functionalization and to evaluate the SARS-CoV-2 antibody−antigen interaction on electrode surfaces. The CVs were performed from −0.3 to +0.8 V and a scan rate of 20 mV/s. Figure 3a shows comparative cyclic voltammograms of the SARS-CoV-2 antibody immunosensor suggesting that the electron transfer kinetics changes from one surface modification step to another. Similarly, for the SARS-CoV-2 antigen immunosensor, the electrochemical analysis is shown in Figure S1. The CV of the bare GCE showed well-defined characteristic redox peaks of ferri/ferrocyanide. The surface modification with GO caused a decrease in peak current values as well as a shift in peak potentials, suggesting that GO had fewer conducting groups. However, the GO−Au modified surface showed a significant increase in peak current and shift in potential due to the highly conducting nature of AuNPs in the GO−Au nanocomposites. Further, in the case of the SARS-CoV-2 antibody immunosensor, the addition of EDC/NHS activated cross-linking groups and supported immobilization of SARS-CoV-2 antigen. This immobilization reduced the electron transfer kinetics due to the presence of insulating protein molecules on the electrode surface, which is seen from the decreased peak current in the CV curve. Further, BSA blocked the unbound electrode surface, hindering the diffusion of the ferri/ferrocyanide redox couple, as evidenced by the low peak current and a potential shift in the CV curve. This suggests the successful fabrication of the SARS-CoV-2 antibody immunosensor. The peak anodic and cathodic currents, along with corresponding potentials, are reported in Table S1.

Subsequently, the Randal−Sevcik equation[32] was used to calculate the effective surface area of the modified electrodes. The corresponding calculations are given below. The peak current (I_p) is expressed as

$$I_p = (2.69 \times 10^5) n^{3/2} A D^{1/2} C v^{1/2} \quad (1)$$

where n is the number of electrons transferred in the redox reaction (here, 1), A is the effective active surface area of the electrode (cm^2), D is the diffusion coefficient ($D = 7.26 \times 10^{-6}$ cm^2/s) for the ferri/ferrocyanide redox solution,[33] C is the concentration of the ferri/ferrocyanide redox solution (here, 5×10^{-6} mol/cm^3), and v is the scan rate (here, 20 mV/s).

For the bare GCE electrode, the I_{p_A} was observed to be 42.95 μA, and the effective surface area was 8.38×10^{-2} cm^2.[31] Subsequently, the active surface areas of the modified electrodes in case of SARS-CoV-2 antibody immunosensor were calculated as $A_{GO} = 6.42 \times 10^{-2}$ cm^2, $A_{GO-Au} = 9.24 \times 10^{-2}$ cm^2, $A_{GO-Au/Ag} = 7.17 \times 10^{-2}$ cm^2, and $A_{GO-Au/Ag/BSA} = 5.27 \times 10^{-2}$ cm^2. In the case of the SARS-CoV-2 antigen immunosensor, the calculations for the respective modified electrodes are shown in the Supporting Information.

Moreover, the scans at rates from 10 to 70 mV/s were conducted in redox electrolyte for the synthesized GO−Au nanocomposites and SARS-CoV-2 antibody immunosensor to evaluate the sensor reversibility. The cyclic voltammograms obtained were symmetric (data not shown) and were further used to plot regression curves of the peak currents obtained in each cycle vs square root of scan rate. The results for SARS-CoV-2 antibody immunosensor, seen in Figure 3c, were linear; that is, the values of anodic peak currents increase with the increase in scan rate, and those of cathodic peak currents decrease with the increase in scan rate, suggesting diffusion-controlled reaction and reversible electron transfer kinetics.[34] The regression curves were used to compare the relation between anodic (I_{p_A}) and cathodic peak currents (I_{p_C}) vs square root of scan rate ($\nu^{1/2}$), which was found to be linear for

https://doi.org/10.1021/acsabm.2c00301
ACS Appl. Bio Mater. 2022, 5, 2421−2430

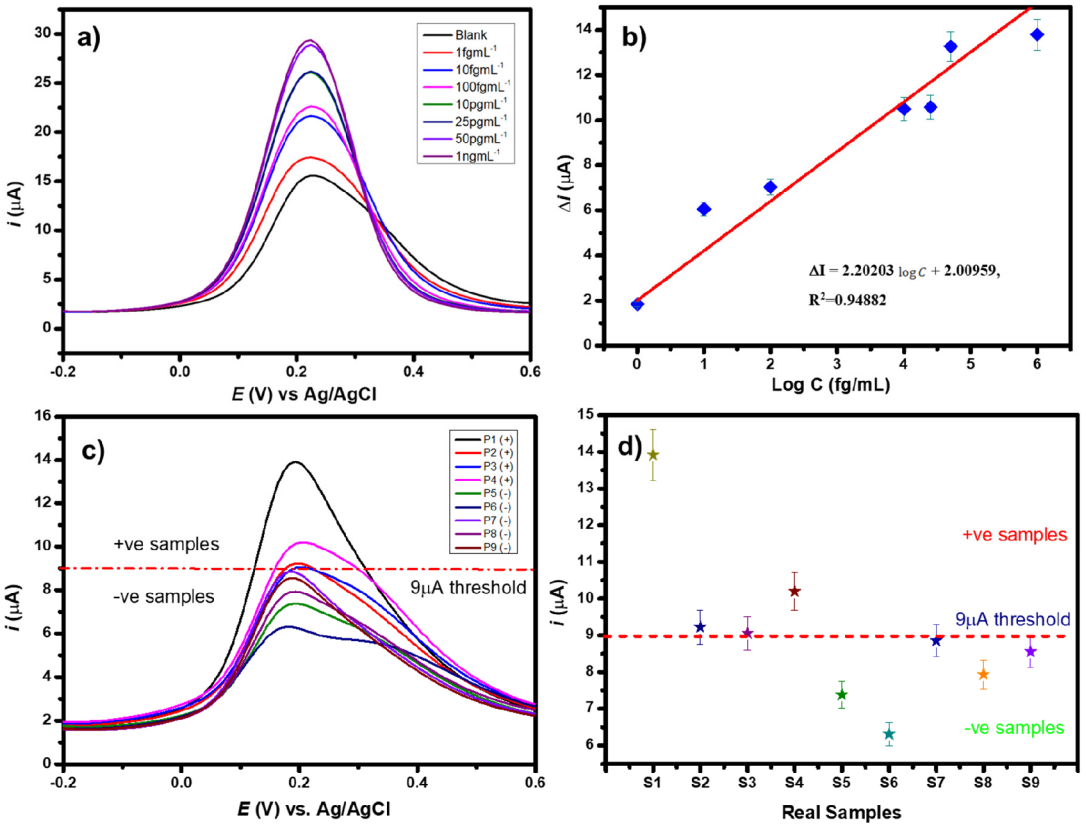

Figure 4. (a) DPV current responses of the SARS-CoV-2 antibody immunosensor with various concentrations of SARS-CoV-2 antibody. (b) Calibration plot of the linear relationship between change in peak current and the log concentrations of SARS-CoV-2 antibody. (c) DPV curve of SARS-CoV-2 antibody detection in patient serum samples. (d) Quantitative screening of positive and negative patient serum samples with a threshold of peak current 9 μA.

the GO−Au nanocomposites as well as fabricated SARS-CoV-2 antibody immunosensor.

$$I_{p_A}(\text{GCE/GO−Au})\ (\mu\text{A}) = 3.93\nu^{1/2}\ (\text{V/s}) + 24.57,\quad R^2 = 0.99099 \tag{2}$$

$$I_{p_C}(\text{GCE/GO−Au})\ (\mu\text{A}) = -6.28\nu^{1/2}\ (\text{V/s}) - 11.11,\quad R^2 = 0.98366 \tag{3}$$

$$I_{p_A}(\text{GCE/GO−Au/Ag/BSA})\ (\mu\text{A}) = 3.56\nu^{1/2}\ (\text{V/s}) + 93.11,\quad R^2 = 0.99521 \tag{4}$$

$$I_{p_C}(\text{GCE/GO−Au/Ag/BSA})\ (\mu\text{A}) = -3.59\nu^{1/2}\ (\text{V/s}) - 18.16,\quad R^2 = 0.97659 \tag{5}$$

The corresponding calculations show excellent linearity, which is supported by the values of respective regression coefficients (R^2). Values for the SARS-CoV-2 antigen immunosensor are reported in the Supporting Information.

The high sensitivity of the DPV technique is observed from one step to another in the modified electrodes, where the GO−Au nanocomposite has the highest peak current and the SARS-CoV-2 antibody immunosensor has the lowest current after BSA blocking. The peak current values and potential shifts are observed at each surface modification step as shown in Table S2. The obtained DPV curves as shown in Figure 3b are consistent with the CV results as discussed above in Figure 3a.

Further EIS data interpretation was done for each step of electrode surface modification. The Nyquist plot, as shown in Figure 3d, displays real and imaginary impedance components as *x*- and *y*-axis, respectively. There is a direct relation of obtained impedance data with frequency. The right portion of the graph with higher impedance values corresponds to low-frequency data, and the left portion of the graph corresponds to higher-frequency data. The semicircle portion of the Nyquist plot obtained at high-frequency values indicates the electron transfer capacity from the surface of the electrode to the ferri/ferrocyanide redox couple solution, commonly referred to as charge transfer resistance, R_{ct}. The straight-line portion of the curve at low-frequency values shows the diffusion-controlled behavior at the planar electrode, which indicates the reaction time. The respective R_{ct} values of each surface-modified electrode are reported in Table S2.

From the Nyquist plot shown in Figure 3d, the bare GCE has a low R_{ct} value (small semicircle) compared to the GO modified working electrode, which can be attributed to the distorted sp^2 network and presence of functional groups that hinder electron transfer.[18,35] The R_{ct} value of the GO−Au nanocomposites is the lowest (smallest semicircle) suggesting the extremely high conducting nature of the GO−Au nanocomposites. After electrode surface modification by SARS-CoV-2 antigen (Ag), the R_{ct} value increased, suggesting successful immobilization of the proteins on the surface. Further, after BSA blocking for unbound sites on the electrode,

https://doi.org/10.1021/acsabm.2c00301
ACS Appl. Bio Mater. 2022, 5, 2421−2430

Table 1. Electrochemical Biosensors for the Detection of SARS-CoV-2 Antibody and Antigen[a]

matrix	detection technique	target analyte	sample	LOD	linear range	ref
graphene	SWV	spike protein	PBS	20 ng mL^{-1}	260−1040 nM	34
Co-TNTs	amperometry	S-RBD protein	buffer solution	0.7 nM	14−1400 nM	36
AuNP−mAb	SWV	spike antigen	PBS	1 pg mL^{-1}	1 pg mL^{-1} to 10 ng mL^{-1}	39
AuNPs	SWV	spike antigen	ferri/ferrocyanide	229 fg mL^{-1}	10 fg mL^{-1} to 1 ng mL^{-1}	40
gold clusters	SWV	spike antibody	saliva and oropharyngeal swab	0.03 fg mL^{-1}	0.1 fg mL^{-1} to 10 pg mL^{-1}	41
Au-based electrode	EIS	antibodies	serum sample	1.99 nM	0−150 nM	42
GO−Au nanocomposites	DPV	SARS-CoV-2 antibody	PBS	1 fg mL^{-1}	1 fg mL^{-1} to 1 ng mL^{-1}	this work
GO−Au nanocomposites	DPV	SARS-CoV-2 antigen	PBS	3.99 ag mL^{-1}	10 ag mL^{-1} to 75 pg mL^{-1}	this work

[a]Abbreviations: Co-TNTs, cobalt-functionalized TiO_2 nanotubes; SWV: Square wave voltammetry.

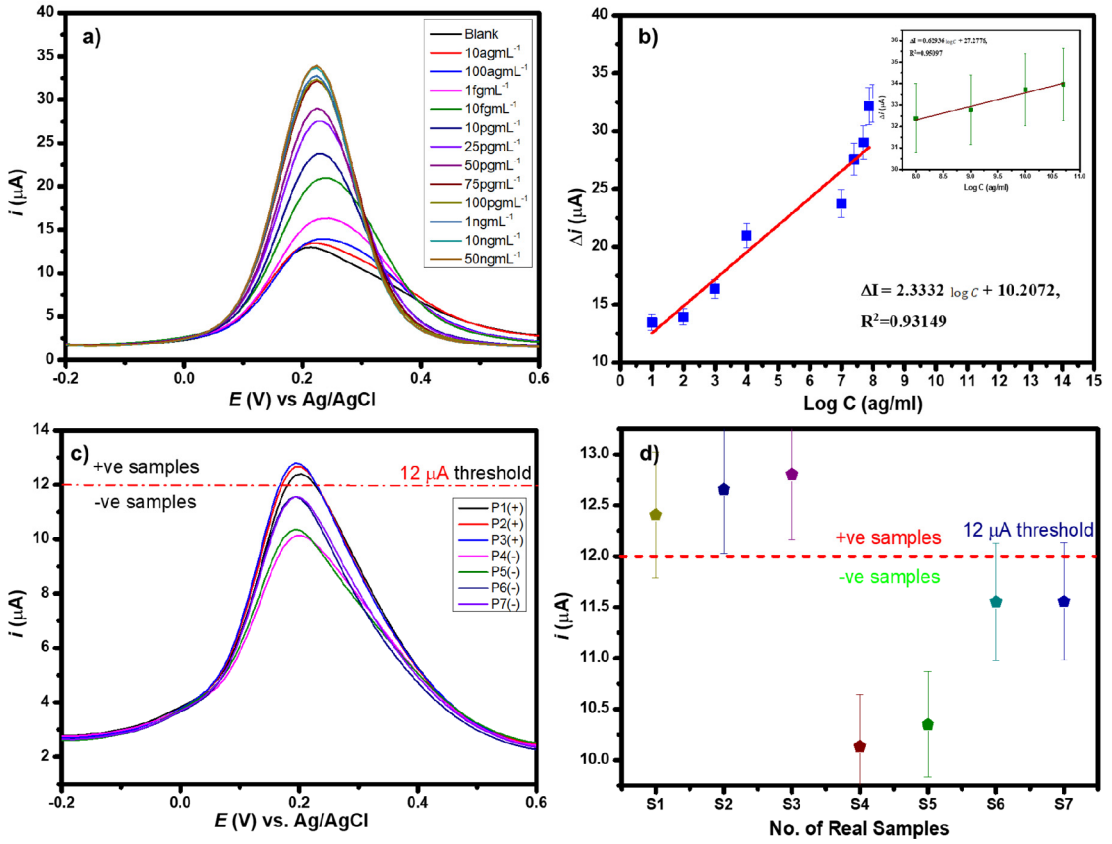

Figure 5. (a) DPV current responses of the SARS-CoV-2 antigen immunosensor with various concentrations of SARS-CoV-2 antigen. (b) Calibration plot of the linear relationship between change in peak current and log concentrations of SARS-CoV-2 antigen. (c) DPV curve of SARS-CoV-2 antigen detection in patient serum samples. (d) Quantitative screening of positive and negative patient swab samples with a threshold of peak current 12 μA.

the R_{ct} was highest (largest semicircle) evidencing the effective blocking of the unbound sites on the electrode surface. The bode plots in Figure 3e,f show the correlation of the phase shift and amplitude with frequency. The GO−Au nanocomposites modified electrode has the smallest phase shift, whereas the fabricated SARS-CoV-2 antibody immunosensor has the largest phase shift. The relevant electrochemical results suggested the successful fabrication of the SARS-CoV-2 antibody immunosensor. These results are consistent with the CV and DPV results.

3.5. Voltammetric Detection of SARS-CoV-2 Antibody. The performance of the fabricated SARS-CoV-2 antibody immunosensor was verified through DPV. The developed SARS-CoV-2 antibody immunosensor was incubated with various concentrations of SARS-CoV-2 antibody from 1 fg mL^{-1} to 1 ng mL^{-1}. The DPV measurements were performed in the −0.3 to +0.8 V potential window. The characteristic peak of the SARS-CoV-2 antibody immunosensor in the absence of SARS-CoV-2 antibody was observed at 0.22 V potential with a peak current of 15.59 μA. As observed from the DPV detection curve (Figure 4a), the current response was directly dependent on the concentration of the SARS-CoV-2 antibody. As the concentration of SARS-CoV-2 antibody increased from 1 fg mL^{-1} to 1 ng mL^{-1}, a corresponding increase in the current intensity was observed. The increase in the current intensity could be attributed to

https://doi.org/10.1021/acsabm.2c00301
ACS Appl. Bio Mater. 2022, 5, 2421−2430

electrochemical activation of the protein molecules that form a complex between the GO−Au nanocomposites and the protein. As the concentration of the SARS-CoV-2 antibody in the solution increased, the formation of the complex led to an increase in electron transfer.[36]

As the SARS-CoV-2 antibody immunosensor was observed to show excellent linearity as seen from Figure 4b for the linear range of 1 fg mL^{-1} to 1 ng mL^{-1}, the limit of detection (LOD) and limit of quantification (LOQ) were calculated from the following equations LOD = (3.3 x SD)/S, LOQ = (10 x SD)/S. The response of the callibration plot is presented in equation 6:

$$\Delta I(\text{antibody immunosensor})\ (\mu A) = (2.20203 \log C\ (\text{fg mL}^{-1}) + 2.00959), \quad R^2 = 0.94882 \tag{6}$$

where SD is the standard deviation of the response of the callibration plot = standard error (SE) of intercept x $N^{1/2}$, N = number of samples, S = slope of the callibration plot. The LOD and LOQ were estimated to be 1 fg mL^{-1} and 3.03 fg mL^{-1}, respectively. The obtained LOD of the fabricated SARS-CoV-2 antibody immunosensor was superior compared to the previously reported sensors. The various electrochemical biosensors for the detection of SARS-CoV-2 antibodies are compared in Table 1.

3.6. Detection of Anti-SARS-CoV-2 Antibody in Patient Serum Samples. The fabricated SARS-CoV-2 antibody immunosensor was further utilized to detect SARS-CoV-2 antibody in patient serum samples. The samples were taken from 9 different patients tested for COVID-19 (4 positives and 5 negatives). The DPV technique was employed to quantify the detection as shown in Figure 4c, where the threshold limit was set to be 9 μA such that the positive samples have higher peak current values than the threshold and negative samples have lower peak current values than the set threshold current. The corresponding screening plot, as seen in Figure 4d, helps to differentiate between positive and negative samples from the given samples effectively. The results reveal the validation of the fabricated SARS-CoV-2 antibody immunosensor for clinical samples. This can further be made portable and commercial for rapid and accurate screening of the patients to handle the ongoing pandemic effectively.

3.7. Voltammetric Detection of SARS-CoV-2 Antigen. A detailed analysis of the electrochemical activity was carried out on a fabricated SARS-CoV-2 antigen immunosensor before utilizing it for detection of the SARS-CoV-2 antigen following the same protocol as that for the SARS-CoV-2 antibody immunosensor. The initial characterization of each fabrication step of the SARS-CoV-2 antigen immunosensor is shown in Figure S1.

To verify the performance of the fabricated SARS-CoV-2 antigen immunosensor, recombinant SARS-CoV-2 antigen was used against the SARS-CoV-2 antibody for electrochemical detection via DPV. The fabricated SARS-CoV-2 antigen immunosensor was incubated with various concentrations of SARS-CoV-2 antigen from 10 ag mL^{-1} to 50 ng mL^{-1}. The potential window for DPV measurements was −0.3 to +0.8 V. The characteristic peak of the SARS-CoV-2 antigen immunosensor without any target analyte was observed at 0.21 V potential with a peak current of 12.98 μA. As observed from the DPV detection curve (Figure 5a), the current response is directly dependent on the concentration of the SARS-CoV-2 antigen. As the concentration of SARS-CoV-2 antigen increased from 10 ag mL^{-1} to 50 ng mL^{-1}, a corresponding increase in the current intensity was seen. This trend in current response can be attributed to an increase in electron transfer between negatively charged ferri/ferrocyanide redox couple and positively charged SARS-CoV-2 antigen attracted toward each other.[37,38]

As seen from Figure 5b, there are two linear relations between the log of concentration and change in current response between 10 ag mL^{-1} to 75 pg mL^{-1} and 100 pg mL^{-1} to 50 ng mL^{-1}. The subsequent regression curve equations are as follows:

$$\Delta I(\text{SARS-CoV-2 antigen immunosensor}\ (\mu A)/(2.3332 \log C\ (\text{ag mL}^{-1}) + 10.2072), \quad R^2 = 0.93149\ \{10\ \text{ag mL}^{-1}\ \text{to}\ 75\ \text{pg mL}^{-1}\} \tag{7}$$

$$\Delta I(\text{SARS-CoV-2 antigen immunosensor})\ (\mu A)/(0.62936 \log C(\text{ag mL}^{-1}) + 27.2776), \quad R^2 = 0.95097\ \{100\ \text{pg mL}^{-1}\ \text{to}\ 50\ \text{ng mL}^{-1}\} \tag{8}$$

As the SARS-CoV-2 antigen immunosensor was observed to show excellent linearity for the linear range of 10 ag mL^{-1} to 75 pg mL^{-1}, the LOD and LOQ were estimated to be 3.99 ag mL^{-1} and 12.09 ag mL^{-1} respectively. The obtained LOD of the fabricated SARS-CoV-2 antigen immunosensor is superior to those from the previously reported studies. The various electrochemical biosensors for the detection of SARS-CoV-2 antigen are compared in Table 1.

3.8. The Detection of SARS-CoV-2 Antigen in Patient Swab Samples. The fabricated SARS-CoV-2 antigen immunosensor was further utilized to detect the SARS-CoV-2 antigen in patient swab samples. The samples were taken from 7 different patients tested for COVID-19 (3 positives and 4 negatives). The DPV technique was employed to quantify the detection Figure 5c, where the threshold limit was set to be 12 μA. The positive samples have higher peak current values than the threshold value, and the negative samples have lower peak current values than the set threshold current. The corresponding screening results have been plotted between the current and number of real samples as seen in Figure 5d, which helped to differentiate between positive and negative samples from the given samples effectively. The results reveal the quantitative performance of the fabricated SARS-CoV-2 antigen immunosensor with patient swab samples and show that the results are consistent with the RT-PCR test. This can further be made portable and commercial for rapid and accurate screening of the patients to handle the ongoing pandemic effectively.

4. CONCLUSION

In summary, we have developed GO−Au nanocomposites-based electrochemical immunosensor platforms for dual detection of SARS-CoV-2 antigen and SARS-CoV-2 antibody. The synthesized GO−Au nanocomposites shows excellent features like high conductivity, good biocompatibility, and high surface functionality. Furthermore, characterization techniques determined the average particle size of the AuNPs to be 12.1 nm, which corresponds to high surface area. The electrochemical studies revealed that the proposed immunosensor platforms have high sensitivity for the detection of SARS-CoV-2 antigen and antibody. The SARS-CoV-2 antigen immunosensor showed excellent sensitivity in the linear range of 10 ag mL^{-1} to 50 ng mL^{-1} with LOD of 3.99 ag mL^{-1}, and the SARS-CoV-2 antibody immunosensor exhibit LOD of 1 fg mL^{-1} in the linear range of 1 fg mL^{-1} to 1 ng mL^{-1}.

https://doi.org/10.1021/acsabm.2c00301
ACS Appl. Bio Mater. 2022, 5, 2421−2430

Furthermore, the detection results for both fabricated immunosensors showed a good correlation with patient serum and swab samples as well. Additionally, the fabricated immunosensors have great potential in the development of POC devices for detection of the SARS-CoV-2 virus in near future.

■ ASSOCIATED CONTENT

Supporting Information

The Supporting Information is available free of charge at https://pubs.acs.org/doi/10.1021/acsabm.2c00301.

Synthesis of graphene oxide, pretreatment of the working electrode, and antigen/antibody immunosensor comparative electrochemical data (PDF)

■ AUTHOR INFORMATION

Corresponding Author

Raju Khan − *Industrial Waste Utilization, Nano and Biomaterials, CSIR - Advanced Materials and Processes Research Institute (AMPRI), Bhopal 462026, India; Academy of Scientific and Innovative Research (AcSIR), Ghaziabad 201002, India;* orcid.org/0000-0002-3007-0232; Email: khan.raju@gmail.com, khan.raju@ampri.res.in

Authors

Mohd. Abubakar Sadique − *Industrial Waste Utilization, Nano and Biomaterials, CSIR - Advanced Materials and Processes Research Institute (AMPRI), Bhopal 462026, India; Academy of Scientific and Innovative Research (AcSIR), Ghaziabad 201002, India*

Shalu Yadav − *Industrial Waste Utilization, Nano and Biomaterials, CSIR - Advanced Materials and Processes Research Institute (AMPRI), Bhopal 462026, India; Academy of Scientific and Innovative Research (AcSIR), Ghaziabad 201002, India*

Pushpesh Ranjan − *Industrial Waste Utilization, Nano and Biomaterials, CSIR - Advanced Materials and Processes Research Institute (AMPRI), Bhopal 462026, India; Academy of Scientific and Innovative Research (AcSIR), Ghaziabad 201002, India*

Firoz Khan − *Department of Biochemistry, All India Institute of Medical Sciences (AIIMS), Bhopal 462020, India*

Ashok Kumar − *Department of Biochemistry, All India Institute of Medical Sciences (AIIMS), Bhopal 462020, India*

Debasis Biswas − *Department of Microbiology, All India Institute of Medical Sciences (AIIMS), Bhopal 462020, India*

Complete contact information is available at: https://pubs.acs.org/10.1021/acsabm.2c00301

Notes

The authors declare no competing financial interest.

■ ACKNOWLEDGMENTS

The authors thank the Director, CSIR-AMPRI, Bhopal, for his encouragement in this work. Raju Khan acknowledges SERB-IRPHA for financial aid for this work under the project IPA/2020/000130. The authors thank CSIR-AMPRI for materials characterization facilities and Dr. Mohd. Ashiq for helping in the TEM work which was perfomed at Analytical HRTEM Laboratory, CSIR-AMPRI, Bhopal supported by CSIR under Facility Creation Project (MLP0110).

■ REFERENCES

(1) Bukkitgar, S. D.; Shetti, N. P.; Aminabhavi, T. M. Electrochemical Investigations for COVID-19 Detection-A Comparison with Other Viral Detection Methods. *Chem. Eng. J.* **2021**, *420*, 127575.

(2) Layqah, L. A.; Eissa, S. An Electrochemical Immunosensor for the Corona Virus Associated with the Middle East Respiratory Syndrome Using an Array of Gold Nanoparticle-Modified Carbon Electrodes. *Mikrochim. Acta* **2019**, *186* (4), 224.

(3) Abubakar Sadique, M.; Yadav, S.; Ranjan, P.; Akram Khan, M.; Kumar, A.; Khan, R. Rapid Detection of SARS-CoV-2 Using Graphene-Based IoT Integrated Advanced Electrochemical Biosensor. *Mater. Lett.* **2021**, *305*, 130824.

(4) Yadav, S.; Sadique, M. A.; Ranjan, P.; Kumar, N.; Singhal, A.; Srivastava, A. K.; Khan, R. SERS Based Lateral Flow Immunoassay for Point-of-Care Detection of Sars-CoV-2 in Clinical Samples. *ACS Appl. Bio Mater.* **2021**, *4* (4), 2974−2995.

(5) Sadique, M. A.; Yadav, S.; Ranjan, P.; Verma, S.; Salammal, S. T.; Khan, M. A.; Kaushik, A.; Khan, R. High-Performance Antiviral Nano-Systems as a Shield to Inhibit Viral Infections: SARS-CoV-2 as a Model Case Study. *J. Mater. Chem. B* **2021**, *9* (23), 4620−4642.

(6) Alafeef, M.; Dighe, K.; Moitra, P.; Pan, D. Rapid, Ultrasensitive, and Quantitative Detection of SARS-CoV-2 Using Antisense Oligonucleotides Directed Electrochemical Biosensor Chip. *ACS Nano* **2020**, *14* (12), 17028−17045.

(7) Torrente-Rodríguez, R. M.; Lukas, H.; Tu, J.; Min, J.; Yang, Y.; Xu, C.; Rossiter, H. B.; Gao, W. SARS-CoV-2 RapidPlex: A Graphene-Based Multiplexed Telemedicine Platform for Rapid and Low-Cost COVID-19 Diagnosis and Monitoring. *Matter* **2020**, *3* (6), 1981−1998.

(8) Imran, S.; Ahmadi, S.; Kerman, K. Electrochemical Biosensors for the Detection of SARS-Cov-2 and Other Viruses. *Micromachines* **2021**, *12*, 174.

(9) Parihar, A.; Ranjan, P.; Sanghi, S. K.; Srivastava, A. K.; Khan, R. Point-of-Care Biosensor-Based Diagnosis of COVID-19 Holds Promise to Combat Current and Future Pandemics. *ACS Appl. Bio Mater.* **2020**, *3* (11), 7326−7343.

(10) Seo, G.; Lee, G.; Kim, M. J.; Baek, S.-H.; Choi, M.; Ku, K. B.; Lee, C.-S.; Jun, S.; Park, D.; Kim, H. G.; Kim, S.-J.; Lee, J.-O.; Kim, B. T.; Park, E. C.; Kim, S. Il. Rapid Detection of COVID-19 Causative Virus (SARS-CoV-2) in Human Nasopharyngeal Swab Specimens Using Field-Effect Transistor-Based Biosensor. *ACS Nano* **2020**, *14* (4), 5135−5142.

(11) Li, Y.; Peng, Z.; Holl, N. J.; Hassan, M. R.; Pappas, J. M.; Wei, C.; Izadi, O. H.; Wang, Y.; Dong, X.; Wang, C.; Huang, Y. W.; Kim, D.; Wu, C. MXene-Graphene Field-Effect Transistor Sensing of Influenza Virus and SARS-CoV-2. *ACS Omega* **2021**, *6* (10), 6643−6653.

(12) Zhou, W.; Gao, X.; Liu, D.; Chen, X. Gold Nanoparticles for in Vitro Diagnostics. *Chem. Rev.* **2015**, *115* (19), 10575−10636.

(13) Fani, M.; Rezayi, M.; Pourianfar, H. R.; Meshkat, Z.; Makvandi, M.; Gholami, M.; Rezaee, S. A. Rapid and Label-Free Electrochemical DNA Biosensor Based on a Facile One-Step Electrochemical Synthesis of RGO−PPy−(L-Cys)−AuNPs Nanocomposite for the HTLV-1 Oligonucleotide Detection. *Biotechnol. Appl. Biochem.* **2021**, *68* (3), 626−635.

(14) Saha, K.; Agasti, S. S.; Kim, C.; Li, X.; Rotello, V. M. Gold Nanoparticles in Chemical and Biological Sensing. *Chem. Rev.* **2012**, *112* (5), 2739−2779.

(15) Sangili, A.; Kalyani, T.; Chen, S.-M.; Nanda, A.; Jana, S. K. Label-Free Electrochemical Immunosensor Based on One-Step Electrochemical Deposition of AuNP-RGO Nanocomposites for Detection of Endometriosis Marker CA 125. *ACS Appl. Bio Mater.* **2020**, *3* (11), 7620−7630.

(16) Zhao, H.; Liu, F.; Xie, W.; Zhou, T. C.; OuYang, J.; Jin, L.; Li, H.; Zhao, C. Y.; Zhang, L.; Wei, J.; Zhang, Y. P.; Li, C. P. Ultrasensitive Supersandwich-Type Electrochemical Sensor for SARS-CoV-2 from the Infected COVID-19 Patients Using a Smartphone. *Sensors Actuators, B Chem.* **2021**, *327*, 128899.

(17) Hashemi, S. A.; Golab Behbahan, N. G.; Bahrani, S.; Mousavi, S. M.; Gholami, A.; Ramakrishna, S.; Firoozsani, M.; Moghadami, M.; Lankarani, K. B.; Omidifar, N. Ultra-Sensitive Viral Glycoprotein Detection NanoSystem toward Accurate Tracing SARS-CoV-2 in Biological/Non-Biological Media. *Biosens. Bioelectron.* **2021**, *171*, 112731.
(18) Yakoh, A.; Pimpitak, U.; Rengpipat, S.; Hirankarn, N.; Chailapakul, O.; Chaiyo, S. Paper-Based Electrochemical Biosensor for Diagnosing COVID-19: Detection of SARS-CoV-2 Antibodies and Antigen. *Biosens. Bioelectron.* **2021**, *176*, 112912.
(19) Ali, M. A.; Hu, C.; Jahan, S.; Yuan, B.; Saleh, M. S.; Ju, E.; Gao, S. J.; Panat, R. Sensing of COVID-19 Antibodies in Seconds via Aerosol Jet Nanoprinted Reduced-Graphene-Oxide-Coated 3D Electrodes. *Adv. Mater.* **2021**, *33* (7), 2006647.
(20) Sengupta, J.; Adhikari, A.; Hussain, C. M. Graphene-Based Analytical Lab-on-Chip Devices for Detection of Viruses: A Review. *Carbon Trends* **2021**, *4*, 100072.
(21) Marcano, D. C.; Kosynkin, D. V.; Berlin, J. M.; Sinitskii, A.; Sun, Z.; Slesarev, A. S.; Alemany, L. B.; Lu, W.; Tour, J. M. Correction to Improved Synthesis of Graphene Oxide. *ACS Nano* **2018**, *12* (2), 2078.
(22) Pal, M.; Khan, R. Graphene Oxide Layer Decorated Gold Nanoparticles Based Immunosensor for the Detection of Prostate Cancer Risk Factor. *Anal. Biochem.* **2017**, *536*, 51−58.
(23) Liu, C.; Wang, K.; Luo, S.; Tang, Y.; Chen, L. Direct Electrodeposition of Graphene Enabling the One-Step Synthesis of Graphene−Metal Nanocomposite Films. *Small* **2011**, *7* (9), 1203−1206.
(24) Li, J.; Lin, R.; Yang, Y.; Zhao, R.; Song, S.; Zhou, Y.; Shi, J.; Wang, L.; Song, H.; Hao, R. Multichannel Immunosensor Platform for the Rapid Detection of SARS-CoV-2 and Influenza A(H1N1) Virus. *ACS Appl. Mater. Interfaces* **2021**, *13*, 22262−22270.
(25) Eissa, S.; Zourob, M. Development of a Low-Cost Cotton-Tipped Electrochemical Immunosensor for the Detection of SARS-CoV-2. *Anal. Chem.* **2021**, *93* (3), 1826−1833.
(26) Ghosh, T. K.; Gope, S.; Rana, D.; Roy, I.; Sarkar, G.; Sadhukhan, S.; Bhattacharya, A.; Pramanik, K.; Chattopadhyay, S.; Chakraborty, M.; Chattopadhyay, D. Physical and Electrical Characterization of Reduced Graphene Oxide Synthesized Adopting Green Route. *Bull. Mater. Sci.* **2016**, *39* (2), 543−550.
(27) Ren, X.; Song, Y.; Liu, A.; Zhang, J.; Yang, P.; Zhang, J.; An, M. Experimental and Theoretical Studies of DMH as a Complexing Agent for a Cyanide-Free Gold Electroplating Electrolyte. *RSC Adv.* **2015**, *5* (80), 64997−65004.
(28) Kumarasamy, J.; Camarada, M. B.; Venkatraman, D.; Ju, H.; Dey, R. S.; Wen, Y. One-Step Coelectrodeposition-Assisted Layer-by-Layer Assembly of Gold Nanoparticles and Reduced Graphene Oxide and its Self-Healing Three-Dimensional Nanohybrid for an Ultrasensitive DNA Sensor. *Nanoscale* **2018**, *10* (3), 1196−1206.
(29) Kumar, A.; Sadanandhan, A. M.; Jain, S. L. Silver Doped Reduced Graphene Oxide as a Promising Plasmonic Photocatalyst for Oxidative Coupling of Benzylamines under Visible Light Irradiation. *New J. Chem.* **2019**, *43* (23), 9116−9122.
(30) Debnath, D.; Kim, S. H.; Geckeler, K. E. The First Solid-Phase Route to Fabricate and Size-Tune Gold Nanoparticles at Room Temperature. *J. Mater. Chem.* **2009**, *19* (46), 8810−8816.
(31) Chan, K. F.; Lim, H. N.; Shams, N.; Jayabal, S.; Pandikumar, A.; Huang, N. M. Fabrication of Graphene/Gold-Modified Screen-Printed Electrode for Detection of Carcinoembryonic Antigen. *Mater. Sci. Eng., C* **2016**, *58*, 666−674.
(32) Devi, R.; Gogoi, S.; Dutta, H. S.; Bordoloi, M.; Sanghi, S. K.; Khan, R. Au/NiFe2O4 Nanoparticle-Decorated Graphene Oxide Nanosheets for Electrochemical Immunosensing of Amyloid Beta Peptide. *Nanoscale Adv.* **2020**, *2* (1), 239−248.
(33) Konopka, S. J.; McDuffie, B. Diffusion Coefficients of Ferri- and Ferrocyanide Ions in Aqueous Media, Using Twin-Electrode Thin-Layer Electrochemistry. *Anal. Chem.* **1970**, *42* (14), 1741−1746.
(34) Mojsoska, B.; Larsen, S.; Olsen, D. A.; Madsen, J. S.; Brandslund, I.; Alatraktchi, F. A. Rapid SARS-CoV-2 Detection Using Electrochemical Immunosensor. *Sensors.* **2021**, *21*, 390.
(35) Hu, Y.; Li, F.; Bai, X.; Li, D.; Hua, S.; Wang, K.; Niu, L. Label-Free Electrochemical Impedance Sensing of DNA Hybridization Based on Functionalized Graphene Sheets. *Chem. Commun.* **2011**, *47* (6), 1743−1745.
(36) Vadlamani, B. S.; Uppal, T.; Verma, S. C.; Misra, M. Functionalized TiO_2 Nanotube-Based Electrochemical Biosensor for Rapid Detection of SARS-CoV-2. *Sensors (Basel).* **2020**, *20* (20), 5871.
(37) Eissa, S.; Alhadrami, H. A.; Al-Mozaini, M.; Hassan, A. M.; Zourob, M. Voltammetric-Based Immunosensor for the Detection of SARS-CoV-2 Nucleocapsid Antigen. *Microchim. Acta* **2021**, *188* (6), 199.
(38) Abrego-Martinez, J. C.; Jafari, M.; Chergui, S.; Pavel, C.; Che, D.; Siaj, M. Aptamer-Based Electrochemical Biosensor for Rapid Detection of SARS-CoV-2: Nanoscale Electrode-Aptamer-SARS-CoV-2 Imaging by Photo-Induced Force Microscopy. *Biosens. Bioelectron.* **2022**, *195*, 113595.
(39) Liv, L.; Yener, M.; Çoban, G.; Can, Ş. A. Electrochemical Biosensing Platform Based on Hydrogen Bonding for Detection of the SARS-CoV-2 Spike Antibody. *Anal. Bioanal. Chem.* **2022**, *414* (3), 1313−1322.
(40) de Lima, L. F.; Ferreira, A. L.; Torres, M. D. T.; de Araujo, W. R.; de la Fuente-Nunez, C. Minute-Scale Detection of SARS-CoV-2 Using a Low-Cost Biosensor Composed of Pencil Graphite Electrodes. *Proc. Natl. Acad. Sci. U. S. A.* **2021**, *118* (30), e2106724118.
(41) Liv, L. Electrochemical Immunosensor Platform Based on Gold-Clusters, Cysteamine and Glutaraldehyde Modified Electrode for Diagnosing COVID-19. *Microchem. J.* **2021**, *168* (May), 106445.
(42) Liustrovaite, V.; Drobysh, M.; Rucinskiene, A.; Baradoke, A.; Ramanaviciene, A.; Plikusiene, I.; Samukaite-Bubniene, U.; Viter, R.; Chen, C. F.; Ramanavicius, A. Towards an Electrochemical Immunosensor for the Detection of Antibodies against SARS-CoV-2 Spike Protein. *J. Electrochem. Soc.* **2022**, *169* (3), 037523.

https://doi.org/10.1021/acsabm.2c00301
ACS Appl. Bio Mater. 2022, 5, 2421−2430